

# Characterisation of severely deformed austenitic stainless steel wire

H. S. Wang<sup>1</sup>, J. R. Yang<sup>1</sup> and H. K. D. H. Bhadeshia\*<sup>2</sup>

The microstructure of 8  $\mu\text{m}$  diameter wire produced by the severe deformation of 316L austenitic stainless steel has been examined using TEM and X-ray diffraction. The deformation imparted amounts to a true strain of 6.3. Data from previous studies on strain induced transformation of this steel have been combined with new results to show that true strains  $>2$  are required in order to observe mechanical stabilisation, i.e. the cessation of martensitic transformation when the martensite/austenite interfaces are unable to propagate through the dislocation debris created in the austenite.

**Keywords:** Martensite, Mechanical Stabilization, Interface structure, Stainless steel

## Introduction

Textiles woven using stainless steel threads have applications requiring softness, flexibility, abrasion resistance and the ability to serve at temperatures as high as 650°C. The woven fabrics are generally made using 316L austenitic stainless steel threads and used, for example, to make mould covers for automotive wind-shield manufacture and generally in glass manufacturing processes. Conveyor belts used in the glass industries sometimes have to be heated in order to avoid thermally shocking hot components, whereas those made using stainless steel fabrics can be used without preheat.

The stainless steel thread is made by drawing 190  $\mu\text{m}$  fully annealed stock to a final diameter of 8  $\mu\text{m}$ , without any intermediate heat treatment. A bundle of thread together with an image of a single, slender fibre are illustrated in Fig. 1.

Previous studies of deformed 316L have indicated that rolling deformation induces the transformation of the austenite into  $\alpha'$  martensite, with the quantity of martensite increasing disproportionately with plastic strain.<sup>1,2</sup> However, the level of plastic strain utilised in the previous work is dwarfed by that used for producing the stainless steel thread, where the true strain amounts to about 6.3. This is interesting from the metallurgical point of view, because theory indicates that whereas the defects created by deformation increase the number density of nucleation sites and therefore promoting nucleation, the movement of the martensite/austenite ( $\alpha'/\gamma$ ) interface is obstructed by the defects. When the strain becomes sufficiently large, it becomes impossible for the interfaces to move, causing the transformation to halt. The phenomenon known as mechanical stabilisation arises because the  $\alpha'/\gamma$  interface must be glissile.<sup>3-12</sup>

The purpose of the present work was therefore to understand the structure of the 316L wire in its heavily deformed state and to interpret the results to see whether mechanical stabilisation sets in at the extraordinarily large strains involved.

## Experimental procedure

Stainless steel (316L) wires with 190  $\mu\text{m}$  diameter in the annealed state are used as the starting material in the manufacturing process. The chemical composition is given in Table 1. The actual annealing temperature is proprietary information but it is in excess of 800°C.

The diameter of the starting 190  $\mu\text{m}$  wires is reduced to 8  $\mu\text{m}$  by cold drawing without any intermediate annealing. Therefore, the true strain is 6.3 and results in the partial transformation of the austenite into ferromagnetic martensite.

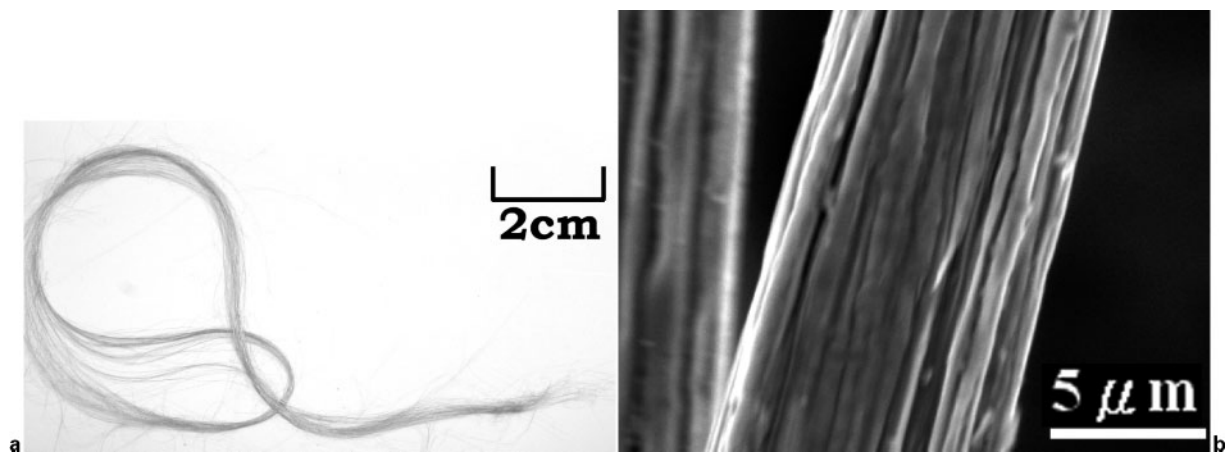
The method by which specimens were prepared from this fine wire for transmission electron microscopy (TEM) analysis is illustrated in Fig. 2. The wire was stretched and mounted between silicon chips using an epoxy adhesive (Epoxy bond 110, Allied High Tech. Products, Inc.) and the assembly cured at 150°C for 15 min before cooling to ambient temperature. The bonded assembly was then affixed to a glass plate using wax (Crystal bond 590, Aremco), heated to 150°C and then cooled to ambient temperature. The specimen-glass set was then thinned by abrasion on silicon carbide paper with 800 and 4000 grit (Fig. 2*b* and *c*), to produce the section illustrated in Fig. 2*d*. The transmitted colour of the silicon ranges from deep red to red, corresponding to thickness ranging from 5 to 10  $\mu\text{m}$ , permitting the thickness to be monitored.<sup>13</sup> After the wire emerges from the thinned wafer, polishing is continued using diamond with particle sizes of 1, 0.5 and 0.1  $\mu\text{m}$ , finishing with 0.06  $\mu\text{m}$  silica wheel.

Interference fringes become visible when the thickness is  $<2$   $\mu\text{m}$  with a yellow transmission colour. The observation of fringes marks the perforation of the foil which is then mounted onto a copper grid (Fig. 2), and

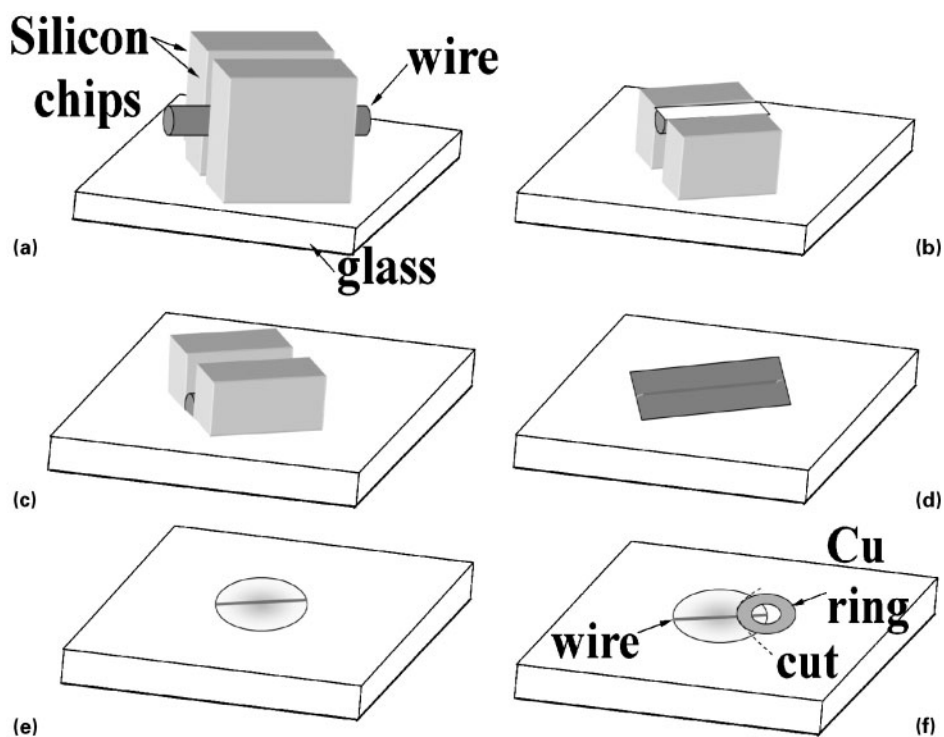
<sup>1</sup>National Taiwan University, Department of Materials Science and Engineering, 1 Roosevelt Road, Section 4, Taipei, Taiwan ROC (106)

<sup>2</sup>Department of Materials Science and Metallurgy, University of Cambridge, Pembroke Street, Cambridge CB2 3QZ, UK

\*Corresponding author, email hkdb@cus.cam.ac.uk



1 *a* Illustration of stainless steel thread bundle in its final form and *b* scanning electron micrograph of individual fibre showing rough surface resulting from drawing operation



2 Illustration of process for preparation of thin foil from 8  $\mu\text{m}$  diameter stainless steel wire

moved into a plasma cleaner for drying and cleaning for TEM analysis. Ion milling was not used in order to avoid the damage of ion bombardment. The foils were examined using JEM 100CX and 2000EX TEM operating at 100 and 200 kV, respectively.

The volume fractions of martensite and austenite were determined using a Bruker AXS Type B8 Advance X-ray diffractometer with the X-ray source of Cu  $K_{\alpha}$  = 1.541 Å operating at 30 kV and 20 mA. The phase fractions were determined taking into account the integrated intensities of (111), (200) and (220) austenite peaks, and of (110), (200), (211) martensite peaks in order to mitigate the effects of crystallographic texture.<sup>14</sup>

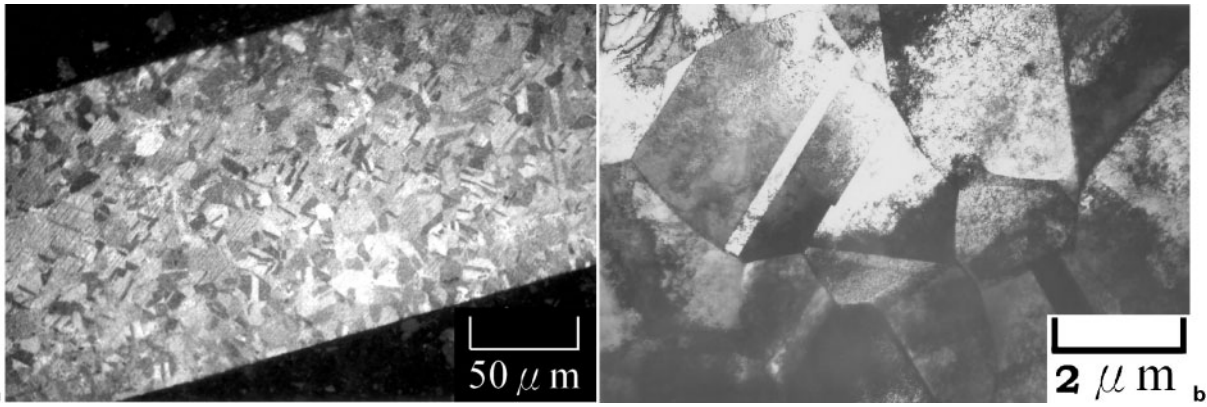
Table 1 Chemical composition of steel used, wt-%

C	Si	Cr	Ni	Mn	Mo	P	S	N	Fe
0.01	0.75	17.1	11.97	0.53	1.99	0.006	0.001	0.046	Bal.

## Microscopy

The initial microstructure of 190  $\mu\text{m}$  diameter wire is presented in Fig. 3. There are equiaxed austenite grains with size of  $\sim 2 \mu\text{m}$  peppered with annealing twins. Although the grains are equiaxed in this annealed sample, Fig. 3 reveals a high dislocation density. It is believed that this is an artifact of the foil preparation technique, which involves grinding and polishing until perforation is achieved.

Figure 4 shows TEM images taken from the transverse and longitudinal sections of the 8  $\mu\text{m}$  diameter wire. The transverse section actually has a very fine grained structure (Fig. 4a). The longitudinal section naturally shows extremely elongated grains owing to the deformation. The combination of micrographs shows that the grains are roughly in the form of prisms elongated in the drawing direction but equiaxed in the cross-section.



a longitudinal section illustrating equiaxed grain structure; b longitudinal section transmission electron micrograph of grain structure

3 190 μm diameter wire

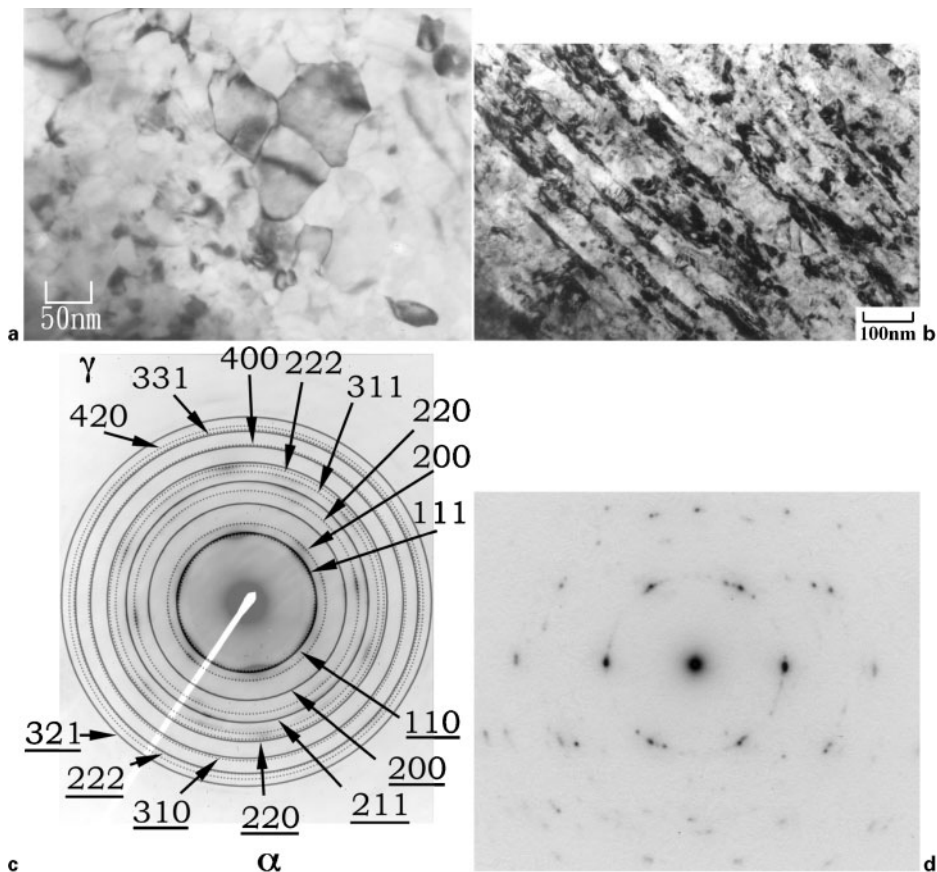
Both the electron diffraction patterns in Fig. 4 are taken using a 2 μm diameter selected area aperture in order to enclose many grains. The electron diffraction pattern from the transverse section (normal to the drawing direction) shows clearly that the material is a mixture of austenite and martensite (Fig. 4c). The pattern is in the form of a ring, consistent with many crystallographic orientations generated by rotation about the longitudinal axis. Not surprisingly, the pattern taken from the longitudinal section, which contains the drawing direction, shows strong crystallographic texture.

Because of the severity of deformation, it is not easy to deduce the individual morphologies of austenite and martensite from the micrographs in Fig. 5. As will be seen later, the martensite appears to form at the early

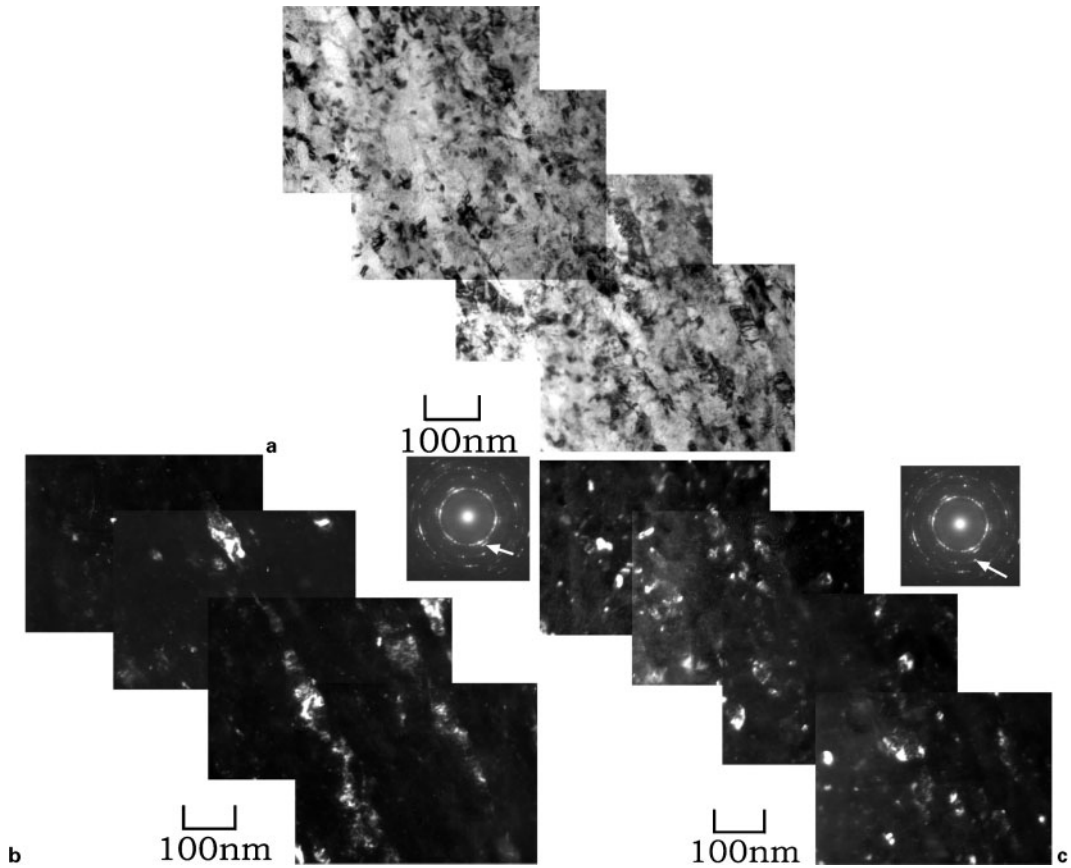
stages of straining and therefore becomes deformed as the drawing operation continues. Therefore, it is not surprising that both the austenite and martensite appear as if they consist of classical dislocation cells. The austenite, being the matrix phase, shows greater continuity, whereas the martensite presumably forms in many variants and therefore appears to be in the form of discrete islands.

Phase fractions

Consistent with the TEM, X-ray analysis of the 190 μm wire indicated that it is fully austenitic (Fig. 6a). The cold reduction by a true strain of 6.3 to the 8 μm thread resulted in the formation of about 57% of α' martensite in the microstructure (Fig. 6b).

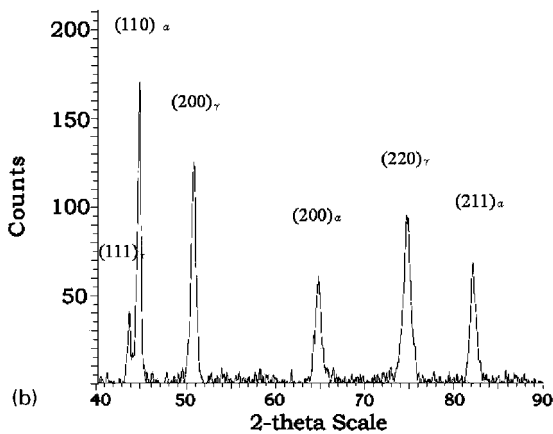
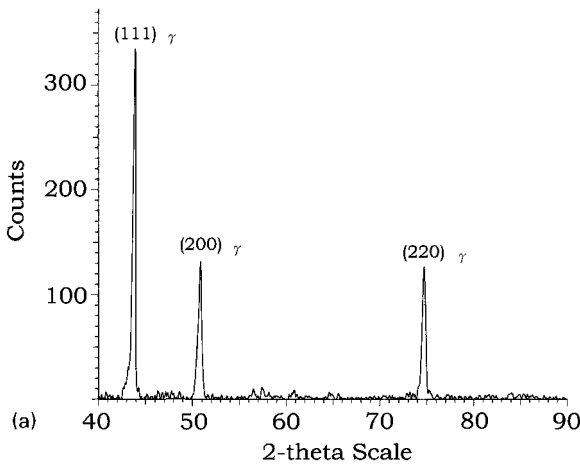


4 8 μm diameter wire



a bright field image; b dark field image of austenite using  $200_\gamma$  reflection; c dark field image of martensite using  $200_\alpha$  reflection

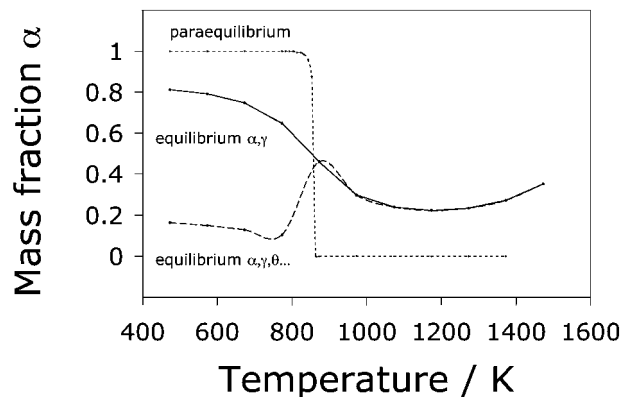
5 Montage of transmission electron micrographs of longitudinal section of wire



6 a diffraction from as received sample and b diffraction from thread

It is well known that stainless steels such as 316L are in a metastable state when they are fully austenitic. Equilibrium requires the presence of ferrite at all temperatures. This is illustrated in Fig. 7, where calculated equilibrium data are presented for a variety of states. The calculations were conducted using MTDATA,<sup>15</sup> which is software capable of accessing thermodynamic data and estimating the equilibrium phase fractions and their chemical compositions as a function of a specified steel composition, set of possible phases, temperature, pressure, etc.; the SGTE database was used in the present work.

It is also possible to do calculations involving constrained equilibria. Paraequilibrium is a state in



7 Calculated ferrite phase fractions for  $\alpha+\gamma$  paraequilibrium,  $\alpha+\gamma$  equilibrium and  $\alpha+\gamma$ +carbides equilibrium

which the substitutional atoms are configurationally frozen; the transformation of austenite to ferrite in these circumstances constrains the substitutional solute to iron atom ratio to be constant everywhere, while carbon partitions to achieve a uniform chemical potential subject to this constraint. It is often the case in steels that paraequilibrium prevails because the mobility of interstitial solute such as carbon is much greater than that of atoms in substitutional sites. Figure 7 shows that 316L steel can become fully austenitic at temperatures  $>863$  K when only paraequilibrium transformation is allowed.

Two further cases are illustrated in Fig. 7, the first case for equilibrium in which only ferrite and austenite are allowed to exist, and the second where cementite and  $M_{23}C_6$  are also allowed to exist. It is clear that neither of the cases can explain the fully austenitic state of the  $190\ \mu\text{m}$  wire. Indeed, equilibrium involving the carbides requires that the ferrite contains huge chromium concentrations at low temperatures, e.g. in excess of 80 wt-% at  $<863$  K. Because this Cr rich ferrite is not found in practice, it is safe to assume that an equilibrium state based on ferrite, austenite and carbides is not representative of commercial 316L.

The corresponding  $\alpha+\gamma$  equilibrium calculations can also be dismissed on the ground that they suggest an excessive quantity of ferrite in the microstructure before deformation (Fig. 7).

Because the  $190\ \mu\text{m}$  wire is found to be fully austenitic, it must be concluded that the paraequilibrium calculations best represent the initial state of the wire. This in turn implies that the processing during manufacture is sufficiently rapid to prevent the diffusion of substitutional solutes, therefore allowing the material to be essentially austenitic in its undeformed state. The initial wire is certainly not at equilibrium, because considerable quantities of ferrite are then expected in the microstructure but not found in practice.

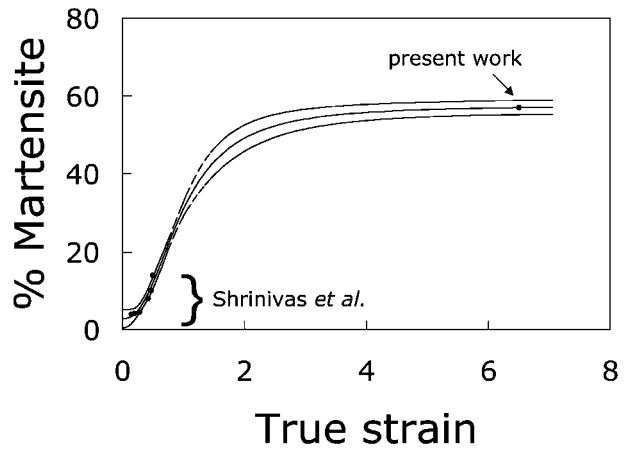
## Evidence for mechanical stabilisation

Martensitic transformation occurs without diffusion, and given the very low carbon concentration in the steel, this is, from a composition point of view, equivalent to saying that it occurs with paraequilibrium. It follows from paraequilibrium that only ferrite is the stable phase at ambient temperature. Therefore it should be possible in principle to completely transform the austenite into martensite.

The fact that only 57% martensite is obtained following severe deformation is proof of the onset of mechanical stabilisation. As explained in the introduction, the  $\alpha'/\gamma$  interface contains glissile dislocations whose motion is hindered or prevented by the presence of defects in the austenite. The retardation of martensitic transformation from plastically deformed austenite has been observed in many systems.<sup>3-12</sup> On the other hand, as shown in Table 2, the data for 316L contradict this statement because an ever increasing martensite content is obtained up to true strains of  $\sim 1$ , with the rate of

**Table 2** Amount of martensite as function of true strain in 316L (data from Refs. 1 and 2), vol.-%

Strain	0.148	0.195	0.278	0.420	0.470	0.995
Martensite	4.0	4.2	4.5	8.0	10.0	14.0



**8** Experimental data (points) and neural network model (solid curve); bounding curves represent  $\pm 1\sigma$  modelling uncertainties

martensite formation rising with strain. This contrasts with mechanical stabilisation reported in 410 stainless steel after a strain of just 0.4.<sup>11</sup>

The present work provides an additional point in the experimental database for 316L, that the amount of martensite for a true strain of 6.3 is 57%. This assumes that the published data,<sup>1,2</sup> which are for rolling deformation, can be compared with our data which are for wire drawing. This may be justified because it is the operation of multiple slip systems and their intersections which stimulate martensite,<sup>2</sup> and multiple slip is inherent in both rolling and drawing.

A neural network technique<sup>16,17</sup> has been used in order to treat the combined dataset and discover the relationship between the martensite fraction and true strain. This method has considerable advantages over normal curve fitting, summarised as follows, with the details described in:

- (i) the fitting function is not a prior assumption as in normal regression analysis but is an outcome of the method
- (ii) the method also provides a modelling uncertainty which indicates the ability of the model to generalise, that is, to make predictions outside of the range of experimental data. The error bar associated with this depends on the position in the input domain where calculations are done. If the calculations are done using inputs where knowledge is sparse, then the indicated uncertainty is large.<sup>16,17</sup>

Figure 8 shows the predicted behaviour alongside the experimental data. It is important to know that the central curve is deduced by the network using procedures which avoid over fitting (fitting to noise in the data); it is not imposed on the data as in normal regression analysis. The two bounding curves represent the modelling uncertainty. It is interesting that the modelling uncertainty is not excessive even in the region where there are no experimental data. This means that the form of the curve is reasonable. Furthermore, the shape is as expected from mechanical stabilisation. There is a region at low strains where martensitic transformation is clearly accelerated by plastic deformation. It is predicted that the austenite becomes mechanically stabilised at a true strain of  $\sim 2$ . This explains why

only 57% martensite is observed with the drawing strain of 6.3, even though the thermodynamic analysis indicates that it should be possible to obtain fully martensitic samples at ambient temperature in principle.

A further implication of mechanical stabilisation at a true strain  $\epsilon=2$  is that any strain beyond 2 will simply deform existing martensite and austenite. This is why the observed morphology of martensite is like austenite, consistent with the deformed state.

Finally, it is worth considering whether the material undergoes dynamic recrystallisation during the course of deformation. The drawing operation is carried out at room temperature and with very high speeds. Therefore, it is unlikely that recrystallisation, which requires diffusion, features in the process. The fact that the material is a two phase mixture also would interfere with any recrystallisation process.

## Conclusions

1. Stainless steel (316L) thread reduced by drawing to 8  $\mu\text{m}$  diameter has a microstructure consisting of strain induced martensite and austenite. The grain structure is strongly textured and is approximated by space filling prisms elongated along the drawing direction in three dimensions.

2. It has been demonstrated that although the austenite can transform completely into martensite under paraequilibrium conditions, it is unable to do so in spite of huge strains, because of the onset of mechanical stabilisation. The stabilisation probably occurs at a strain of 2, so that the subsequent drawing simply deforms the existing mixture of martensite and austenite.

3. The work suggests further experiments, in which the evolution of martensite is studied in the range  $\epsilon=1.5$

to 3. It would also be interesting to study the evolution of microstructure when the deformation is carried out at a lower temperature where the driving force for transformation is greater; the onset of mechanical stabilisation should then occur at a greater strain.

## Acknowledgements

The authors are grateful to the National Science Foundation (Taiwan, ROC) and the Royal Society (UK) for partly funding this research.

## References

1. S. K. Varma, J. Kalyanam and L. E. Murr: *J. Mater. Sci. Letters*, 1994, **13**, 107–111.
2. V. Shrinivas, S. K. Varma and L. E. Murr: *Metall. Mater. Trans. A*, 1995, **26A**, 661–671.
3. J. F. Breedis and W. D. Robertson: *Acta Metall.*, 1963, **11**, 547–559.
4. R. Lagneborg: *Acta Metall.*, 1964, **12**, 823–843.
5. J. R. Strife, M. J. Carr and G. S. Ansell: *Metall. Trans. A*, 1977, **8A**, 1471–1484.
6. J. R. C. Guimares and J. C. Gomes: *Mater. Sci. Eng.*, 1979, **39**, 187–191.
7. K. Tsuzaki, S. Fukasaku, Y. Tomota and T. Maki: *Mater. Trans. JIM*, 1991, **32**, 222–228.
8. Ch. Maier, O. Blaschko and W. Pichl: *Phys. Rev. B*, 1995, **52**, 9283–9290.
9. J. R. Yang, C. Y. Huang, W. H. Hsieh and C. S. Chiou: *Mater. Trans. JIM*, 1996, **37**, 579–585.
10. X. Song, N. Gu and H. Peng: *Defect Diffus. Forum*, 1997, **148–149**, 165–167.
11. M. C. Tsai, C. S. Chiou, J. S. Du and J. R. Yang: *Mater. Sci. Eng.*, 2002, **A332**, 1–10.
12. H. K. D. H. Bhadeshia: *Mater. Sci. Eng. A*, 2004, **A378**, 34–39.
13. J. P. McCaffrey and J. Hulse: *Micron*, 1998, **29**, 139–144.
14. M. J. Dickson: *J. Appl. Crystallogr.*, 1969, **2**, 176–180.
15. 'MTDATA', National Physical Laboratory, Teddington, London.
16. D. J. C. MacKay: *Neural Comput.*, 1992, **4**, 415–472.
17. H. K. D. H. Bhadeshia: *ISIJ Int.*, 1999, **39**, 966–979.